Thermoelectric properties of conducting polymers: The case of poly(3-hexylthiophene)

Y. Xuan,[1] X. Liu,[2] S. Desbief,[3] P. Leclère,[3] M. Fahlman,[2] R. Lazzaroni,[3] M. Berggren,[1] J. Cornil,[3] D. Emin,[4] and X. Crispin[1]
[1]*Department of Science and Technology, Campus Norrköping, Linköping University, S-60174 Norrköping, Sweden*
[2]*Department of Physics, Chemistry and Biology, Linköping University, S-58183 Linköping, Sweden*
[3]*Service de Chimie des Matériaux Nouveaux, Université de Mons (UMONS), Place du Parc 20, B-7000 Mons, Belgium*
[4]*Department of Physics and Astronomy, University of New Mexico, Albuquerque, New Mexico 87131, USA*
(Received 16 March 2010; revised manuscript received 6 September 2010; published 30 September 2010)

Conducting polymers have recently been suggested as thermoelectric materials for use in large-area thermogenerators. To help assessing the feasibility of this the electrical conductivity and Seebeck coefficient of a series of heavily doped regioregular poly(3-hexylthiophene) films are measured between 220 and 370 K. *p*-type chemical doping of up to 34% is accompanied by the introduction of negatively charged counterions, PF_6^-. The counterions produce a disordered environment within which the *p*-type electronic carriers move. This disorder diminishes with increasing doping as the effect of the counterions is smoothed out. Concomitantly the thermally activated electrical conductivity rises strongly while its activation energy decreases. On the other hand, the Seebeck coefficient is found to be weakly dependent on temperature and it decreases with increasing doping. When combined, these results indicate that the thermoelectric power factor reaches a broad maximum between 20% and 31% doping. These results are discussed in terms of the thermally activated hopping-type mobility of bipolarons, deduced from the absence of electron spin resonance signal in the heavily doped materials.

DOI: 10.1103/PhysRevB.82.115454 PACS number(s): 73.61.Ph, 74.25.fg, 71.23.An, 72.20.Pa

I. INTRODUCTION

An ever widening range of materials are being scrutinized for use in Peltier cooling and thermoelectric power generation. The potential of a material for use in these thermoelectric applications is measured by the dimensionless product of its mean operating temperature T and its thermoelectric figure of merit, Z, at this temperature. Efficient devices require materials whose values of ZT are at least close to unity. Expressed in terms of the material transport coefficients

$$ZT = S^2\sigma T/\kappa, \tag{1}$$

where S, σ, and κ denote the material Seebeck coefficient, electrical conductivity, and thermal conductivity, respectively. The Seebeck coefficient, $S=\Delta V/\Delta T$, is the electromotive force ΔV generated across a material when it is subjected to the temperature difference ΔT.

To date, the thermoelectric properties of only a few conjugated polymers have been studied. Table I summarizes the results for eight polymers including polyacetylenes, polyanilines, polypyrroles, poly(paraphenylvinylene), and polythiophenes.[8–12] The electrical conductivities and Seebeck coefficients span very broad ranges: 10^{-5} S/cm to 11 000 S/cm and 7–230 μV/K, respectively.[1–5,7,13–15] The potential for polymeric semiconductors to yield large values of ZT is demonstrated by the findings for polyacetylene samples despite this material not being air stable.

These relatively large values of ZT are fostered by the extremely low thermal conductivities of conducting polymers ($\sim$0.1 W/mK, see Table I), compared to good inorganic thermoelectric substances such as Bi_2Te_3 with $\kappa \sim 1.2$ W/mK.[16] These very low thermal conductivities are comparable to those of phonons of characteristic frequency ν whose mean-free paths are reduced to just a, the minimum separation between equivalent structural units: $k\nu/a$, where k represents the Boltzmann constant. While such low thermal conductivities are common for polymers, they are only found for very complex and disordered inorganic materials.[5,17] By itself, this distinctive feature promotes polymeric semiconductors as materials for thermoelectric applications.

Doping can be exploited to maximize ZT. To begin one can investigate how doping maximizes the thermoelectric power factor $S^2\sigma$, the numerator of Z. Charge carriers added to an insulator generally increase its electrical conductivity and decrease its Seebeck coefficient, the entropy transported by a charge carrier divided by its charge q. The decrease in the Seebeck coefficient with increasing carrier density occurs because the entropy change associated to adding a carrier is reduced as the density of sites already occupied by indistinguishable carriers rises. The competition between the effects of doping on the two factors that define the thermoelectric power factor generally results in it being maximized at a moderate carrier density.

Here we systematically investigate the effects of *p*-type doping on the thermoelectric properties of regioregular poly(3-hexylthiophene) (rr-P3HT). This polymer exhibits a hole mobility ranging from 10^{-5} to 0.1 $cm^2\ V^{-1}\ s^{-1}$ depending on the level of doping impurities.[18] Electrochemical or chemical doping of this polymer increase its electrical conductivity by several orders in magnitude.[19–21] Infrared spectroscopy and electron spin resonance (ESR) measurements indicate polaron formation at very low doping levels and bipolaron formation at higher doping levels.[22,23] We describe the doping-induced evolution of the polymer electrical conductivity and Seebeck coefficients in terms of simple models of thermally assisted polaron and bipolaron hopping.[24–29]

II. METHODOLOGY

A. Experimental approach

A sample of rr-P3HT (98.5% purity) purchased from Aldrich Corporation was dissolved in chloroform at room tem-

TABLE I. The electrical conductivity, Seebeck coefficient, thermal conductivity, and thermoelectric figure of merit of a few polymers.

Polymer	Conductivity σ (S/cm)	Seebeck coefficient S (μV/K)	Thermal conductivity κ (W/mK)	Thermoelectric figure of merit ZT at 300 K
Polyacetylene (Refs. 1–5)	11110	28.4	0.7	3.8×10^{-1}
	11560	11.4		6.9×10^{-2}
	6405	20.6		1.1×10^{-1}
	7530	15.3		7.3×10^{-2}
	4990	14.8		4.7×10^{-2}
Polypyrrole (Refs. 1–5)	100	12	0.1–0.2	2.0×10^{-3}
PEDOT:PSS (Ref. 6)	55	13		1.4×10^{-3}
Polythiophene (Refs. 1–5 and 7)	100	21		6.6×10^{-3}
Poly(carbazolenevinylene) derivative (Refs. 1–3)	5×10^{-3}	230		8.0×10^{-5}
Polyaniline (Refs. 1–5)	7000	7		5.1×10^{-2}
Poly (paraphenylene) (Refs. 2 and 3)	10^{-5}	12		2.1×10^{-10}
Poly(p-phenylenevinylene) (Refs. 1–3 and 5)	10^{-5}	7		7.2×10^{-11}

perature to produce a 5mg/ml solution. Films of P3HT having thicknesses of about 1 μm (measured by microscopy and with a DekTak profilometer) were formed by drop casting this solution on transparent-glass substrates. These glass slides were previously patterned with four gold electrode stripes (50-mm-long, 1-mm-wide, 1-μm-high, and 1 mm spatial interval between each other). These gold stripes serve as electrodes for electrical transport measurements.

The polymer films were doped by immersion in a freshly prepared 0.001 M $NOPF_6$/acetonitrile solution for a prescribed time interval. Each sample was then immediately rinsed in acetonitrile to wash out the remaining $NOPF_6$ salt. The samples were finally dried in a nitrogen flow. Since P3HT is not soluble in acetonitrile, this doping process preserves film homogeneity while eliminating the reduced charge-transfer reaction species (NO). The film soaking time determines its doping level. The doping level was measured with XPS from the ratio of the intensities of the P($2p$) signal from PF_6^- counterions and the S($2p$) signal from P3HT. The intensities were corrected for the transmission function of the spectrometer and cross-section effects.

The photoelectron spectroscopy measurements were performed using an ESCA Scienta 200 spectrometer. The spectrometer is equipped with a monochromatized Al(K_α) x-ray source ($h\nu$=1486.6 eV) with a base pressure of 1×10^{-10} mbar. The energy resolution obtained with the chosen experimental conditions is such that the full-width at the half-maximum of the gold, Au($4f_{7/2}$), line is 0.65 eV. UV-Vis-NIR absorption spectra of the films were recorded at room temperature under air using a Perkin-Elmer Lambda 9 spectrophotometer unit.

Electrical conductivity and Seebeck coefficients were measured in the dark and under vacuum (1×10^{-6} Torr) to eliminate artifacts from photocurrents and photooxidation. Standard four-probe electrical-conductivity measurements utilized a Keithley 2400 digital multimeter maintained at room temperature. The Seebeck coefficient was measured with the sample mounted between two copper blocks separated by 5 mm. One block was in contact with the chuck of a cryonic probe station whose temperature was controlled. The other copper block was thermally insulated from the cryonic probe chuck and heated with an embedded resistance heater. The difference in temperature between the two copper blocks, typically 10 °C, was measured with a digital thermometer. Thermocouples (type K), buried in each of the copper blocks, were placed close to the polymer film while the voltage difference was read with a high precision nanovoltmeter (Keithley Instruments, Inc., model 1282A). The measurements were computer controlled with a general purpose interface bus. Unipolar errors and off-set voltages were eliminated by reversing the polarity of each Seebeck measurement.

B. Theoretical framework

Charge carriers in significantly doped rr-P3HT are believed to form molecular bipolarons. This situation is described with the Holstein-Hubbard model of bipolaron formation in an ideal nonpolar molecular crystal. Here the resulting electrical conductivity and Seebeck coefficient are described.

1. Electrical conductivity

With no more than two carriers permitted to occupy a site, the net concentration of c charge carriers per site comprises a concentration of c_b bipolarons and c_p polarons

$$c = 2c_b + c_p. \tag{2}$$

For definiteness consider the Holstein-Hubbard model of bipolaron and polaron formation in a molecular crystal. The energy of a polaron is defined as $E_1 \equiv -E_b$, where E_b is the lowering of a molecule's energy resulting from atomic rearrangements that accompany its being occupied by a single carrier. Similarly, the energy of a bipolaron is $E_2 \equiv -4E_b + U$, where the lowering of a molecule's energy from atomic rearrangements resulting from a molecule being occupied by two carriers is four times that for a singly occupied molecule and U is the Coulomb repulsion energy between two electronic charges in the bipolaron. Bipolaron formation is ener-

getically favorable when its energy is lower than the net energy of two separated polarons: $2E_1 > E_2$. The energy needed to decompose a bipolaron into two separated polarons is then

$$\varepsilon_b \equiv 2E_1 - E_2 = 2E_b - U. \tag{3}$$

Carriers will tend to amalgamate to form bipolarons when $\varepsilon_b > 0$. Nonetheless an increasing fraction of bipolarons decomposes into polarons as the thermal energy kT is raised.[25] In particular, for $c \ll 1$ the polaron concentration becomes

$$c_p \cong \frac{\sqrt{1 + 2c(e^{\varepsilon_b/kT} - 1)} - 1}{e^{\varepsilon_b/kT} - 1}. \tag{4}$$

Thus, when the carrier concentration c and pair-breaking energy ε_b are large enough so that $2c[\exp(\varepsilon_b/kT) - 1] \gg 1$

$$c_p \cong \sqrt{2c}\, \exp(-\varepsilon_b/2kT). \tag{5}$$

However when $2c[\exp(\varepsilon_b/kT) - 1] \ll 1$, most carriers form polarons $c_p \approx c$.

Molecular bipolarons, such as molecular polarons, often move by thermally assisted hopping. Above a small fraction of the temperature characterizing molecular vibrations polaron-hopping processes follow an Arrhenius-type behavior.[29] The corresponding jump rates and activation energies can then be calculated classically. Bipolarons are found to predominantly hop by decomposing into polarons, hopping, and subsequently reforming as bipolarons.[25] The electrical conductivity for nearest-neighbor hopping is then proportional to the concentration of polarons c_p and to the polaron hopping rate R_p

$$\sigma \cong \frac{Nq^2a^2}{kT} c_p R_p. \tag{6}$$

Here N is the density of sites between which polarons of charge q move and a is their characteristic hopping distance, $Na^2 \sim 1/a$.

The semiclassical polaron jump rate can be written as

$$R_p = \nu e^{-((E_b/2) - t)/kT} P, \tag{7}$$

where ν is the frequency characterizing the vibrations with which the carrier interacts, t is the electronic transfer energy linking the sites between which the polaron hops, and P is the probability that the electron carrier will hop between sites when vibrations establish a transient coincidence between their electronic energies.[28,29] When the electronic transfer energy t is large enough, typically at least comparable to the vibration energy $h\nu$, $P \approx 1$. The electronic carrier is then able to adiabatically follow atomic vibrations and thereby avail itself of every opportunity to negotiate a hop.[27] Alternatively, when the electron transfer energy is very small, hopping becomes nonadiabatic with $P \ll 1$. Then P is proportional to the square of its electronic transfer energy which governs a carrier's hop.

Inserting Eqs. (3), (5), and (7) into Eq. (6) yields an expression for the conductivity for bipolaron hopping among degenerate states

$$\sigma = \frac{Nq^2a^2}{kT} c_p R_p = \frac{Nq^2a^2\nu}{kT} \sqrt{2c} P e^{-E_A/kT}, \tag{8}$$

where the activation energy $E_A \equiv 3E_b/2 - U/2 - t$ is the sum of that for breaking bipolaron pairs and that for polaron hopping. Equation (8) applies to semiclassical bipolaron hopping in an ordered system.

With the imposition of disorder transport becomes increasingly tenuous, disorder creates dispersion among (1) sites occupation probabilities and (2) phonon-assisted intersite jump rates. Nonetheless, the electrical conductivity can retain the general form

$$\sigma = \sigma_o e^{-E/kT}. \tag{9}$$

With increasing disorder the activation energy E rises while the pre-exponential factor σ_o decreases.

2. Seebeck coefficient

The Seebeck coefficient of a charge carrier is the entropy transported with it divided by its charge q. Most often the transported entropy is taken to be just the change in the entropy of mixing associated with adding a carrier to equilibrated carriers distributed among thermally accessible conducting states. With no more than two carriers permitted on any of the equivalent sites, most carriers will pair as bipolaron $c_b \approx c/2$ when $\varepsilon_b \gg kT$ to give a Seebeck coefficient of

$$S \cong \frac{k}{2q} \ln\left(\frac{1 - c_b}{c_b}\right) + \frac{k}{q} \frac{\left(\frac{1}{2} - c_b\right)}{\sqrt{c_b(1 - c_b)}} \left(\frac{\varepsilon_b}{2kT}\right) e^{-\varepsilon_b/2kT}. \tag{10}$$

Here the first contribution is from singlet-paired carriers of charge $2q$ and the second contribution is from thermally-induced broken pairs.[25] Both contributions change sign at $c_b = \frac{1}{2}$.

In the limit that all carriers form bipolarons $\varepsilon_b \to \infty$ with no more than one bipolaron per site, Fermi-Dirac statistics can be employed to write the bipolaron concentration in terms of the bipolaron energy E_2 and the carrier chemical potential μ

$$c_b = \frac{1}{e^{(E_2 - 2\mu)/kT} + 1}. \tag{11}$$

In this limit the Seebeck coefficient is expressed in terms of the bipolaron energy E_2

$$S = \frac{k}{2q}\left(\frac{E_2 - 2\mu}{kT}\right). \tag{12}$$

With energetic disorder at sites with equivalent electron-phonon interactions the net Seebeck coefficient for hopping conduction is an average of the Seebeck coefficient for each hop weighted by its contribution to the thermally activated conductivity.[24] This average Seebeck coefficient has the form[26]

$$S = \frac{k}{2q}\left[\left(\frac{E_2^{min} - 2\mu}{kT}\right) + \left\langle \frac{E_2 - E_2^{min}}{kT} \right\rangle_\sigma\right] \equiv \frac{k}{2q}\left[\left(\frac{E_2^{min} - 2\mu}{kT}\right) + A(T)\right], \quad (13)$$

where $A(T)$ is nearly a constant whose value rises with the density of localized states between which carriers hop, provided that the disorder-induced width of this band of states exceeds kT.[26] The value of this constant often exceeds the value of A, the so-called heat-of-transport constant, found for extended-state motion in conventional wide-band crystalline semiconductors, $A \sim 1-2$.

The Seebeck coefficient is most usefully described by Eqs. (12) and (13) when the chemical potential is "pinned" (i.e., independent of temperature) and carriers are generated by exciting them from valence bands, traps, or dopants. In these instances the magnitude of the Seebeck coefficient decreases with increasing temperature. By contrast, Eq. (10) is often employed when carriers are produced directly by doping. In these instances the Seebeck coefficient is nearly temperature independent.

III. RESULTS AND DISCUSSION

A. Chemical insight into the doping reaction

When the pristine P3HT film is dipped into the dopant $NOPF_6$/acetonitrile solution, NO^+ cations and PF_6^- anions diffuse into the film. During the oxidation NO^+ cations which capture electrons from P3HT and leave the film as NO gas molecules. The resulting positive charges on the polymer chains are balanced by the presence of PF_6^- counter-ions. Since a NO^+ can accept only one electron, this process proceeds by one-electron transfer rather than by the two-electron transfer found in electrochemical doping.[21]

The Single or double charges and their associated structural relaxations (extending about 3–6 monomer units) constitute positive polarons and bipolarons. Figure 1 illustrates the oxidation processes forming polarons and bipolarons on rr-P3HT. Infrared spectroscopy indicates that the neutral state of P3HT has an aromatic character which acquires a quinoid character when polarons and bipolarons are formed.[22] Polarons are only observed in lightly doped P3HT (0.06% with $\sigma = 10^{-4}$ S/cm) where they produce an asymmetric ESR signal.[23] As the dopant level increases, the ESR signal vanishes as polarons are replaced by singlet bipolarons.

The evolution of the absorption spectra of polymer films with increasing exposure to $NOPF_6$ is shown in Fig. 2. The isosbestic point observed at 632 nm indicates the transformation between coexisting (1) neutral and (2) charged polymer species. With progressively increased doping, (1) the oscillator strength of interband (HOMO-LUMO: highest occupied molecular orbital-lowest unoccupied molecular orbital) transition from the pristine P3HT decreases while (2) the intensity of the subgap electronic transition (associated with the presence of bipolarons in the doped material) increases.[30–33] In particular, the absorption of the neutral polymer chains (at 557 nm) decreases continuously and is blueshifted to 530 nm

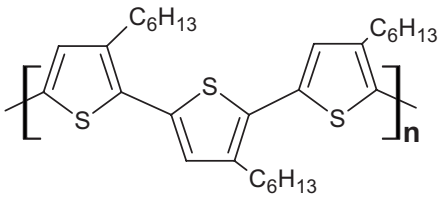

Neutral P3HT

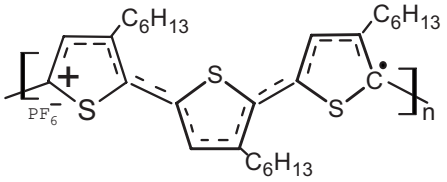

Polaron

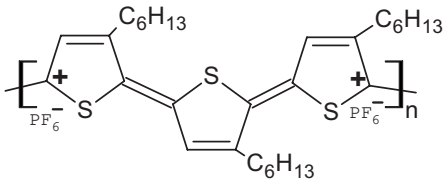

Bipolaron

FIG. 1. Chemical sketches of the pristine, singled-charged (polaron), and doubly charged (bipolaron) poly (3-hexylthiophene) with their counterions. The chemical reaction of the doping reaction is: $P3HT + NOPF_6 \rightarrow NO + P3HT^+(PF_6)^-$.

as doping is increased. At high-enough doping, the shoulder at 605 nm, attributed to P3HT chains that are stacked by π-π interactions disappears.[20,34] Meanwhile increased doping causes the progressive emergence of two new absorption features below the gap edge: a peak around 795 nm and a broad absorption in the 1100–3000 nm range. The appearance of

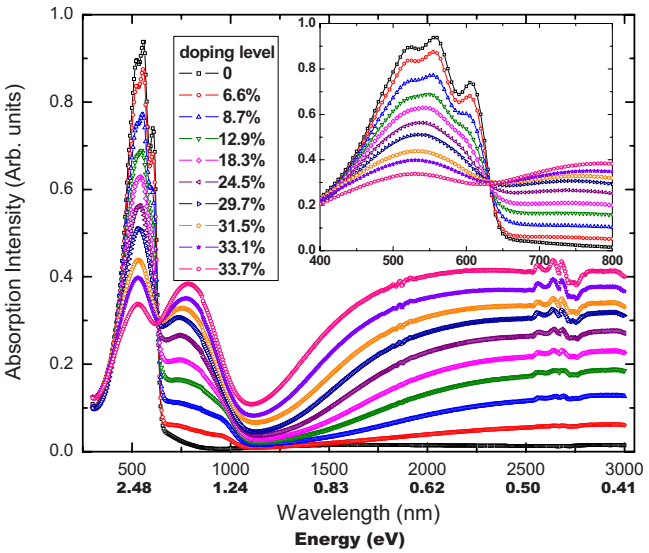

FIG. 2. (Color online) Evolution of the optical-absorption spectrum of P3HT as a function of doping level. Inset is a graph zoom in from 400 to 800 nm.

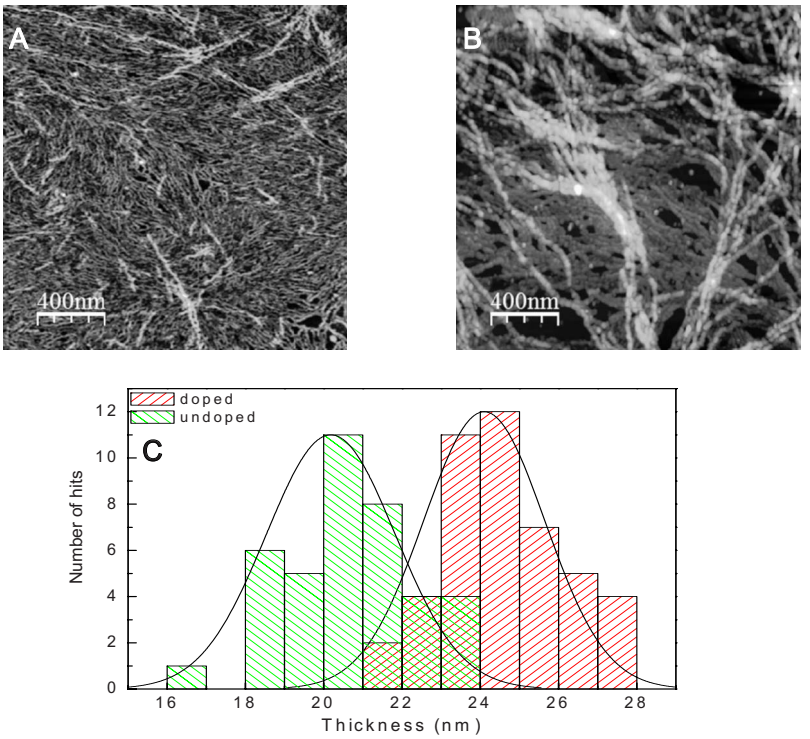

FIG. 3. (Color online) 2×2 μm^2 height AFM images of P3HT films (A) undoped, (B) doped with a 0.5 mg/mL $NOPF_6$ solution in acetonitrile. (C) Distribution of the fibril width for the undoped (green downward diagonal) and doped (red upward diagonal) deposits.

these two subgap absorption bands has been attributed to doping introducing carriers that pair as interacting bipolarons while reducing the HOMO-LUMO energy gap.[35,36]

Doping also affects the film morphology. Figures 3(a) and 3(b) show atomic force microscopy images (2×2 μm^2) of P3HT before and after doping, respectively. The deposits are made of thin long fibrils which result from P3HT chains forming π-π stacks.[37] The fibrillar structure is preserved upon doping even though the doping process occurs in a liquid phase which could have disrupted the thinnest deposits. This observation is crucial since this particular fibrillar structure is expected to be very favorable for charge transport. The histogram in Fig. 3(c) shows the fibril width distribution before and after doping. The average width of 20.2 nm for the undoped fibrils is consistent with the length of extended P3HT chains π stacked perpendicular to the fibril axis. The doped fibrils (~33% doping level) are wider by about 4 nm. We hypothesize that the PF_6^- ions incorporated next to the conjugated backbone lead to some lateral shift of the polymer chains with respect to each other, which in turn induces a broadening of the assembly. Hence, the chemical doping affects the chain assembly, likely alter the electronic coupling between adjacent chains, but does not destroy the self-assembled P3HT nanofibers.

While the morphology of the doped P3HT films displays spatial molecular order, the energies of bipolaron sites experience doping-induced disorder. This disorder arises in part from electrostatic interactions of those sites with surrounding irregularly placed localized charge carriers and PF_6^- counterions.[7] Disorder also results from grain boundaries or amorphous domains between P3HT fibers. We can thus conclude that doping produces positively charged bipolarons within an energetically disordered environment.

B. Electrical conductivity

The electrical conductivity was measured between 220 and 370 K on a series of samples in between 0% (pristine) and 34% of doping. As shown in Fig. 4, the conductivity is thermally activated in all samples. As plotted in Fig. 5, the activation energy is related to the doping level: 0.142 eV, 0.109 eV, 0.075 eV, and 0.036 eV for 0% (pristine), 9%, 25%, and 34% intentional doping, respectively. Figure 5 also shows that the magnitude of the conductivity pre-exponential factor rises strongly with increasing doping. At the highest doping level, the value of the pre-exponential factor is comparable to that expected for adiabatic hops ($P\approx1$).

The steep rise of the pre-exponential factor of the electrical conductivity with increasing dopant level indicates that

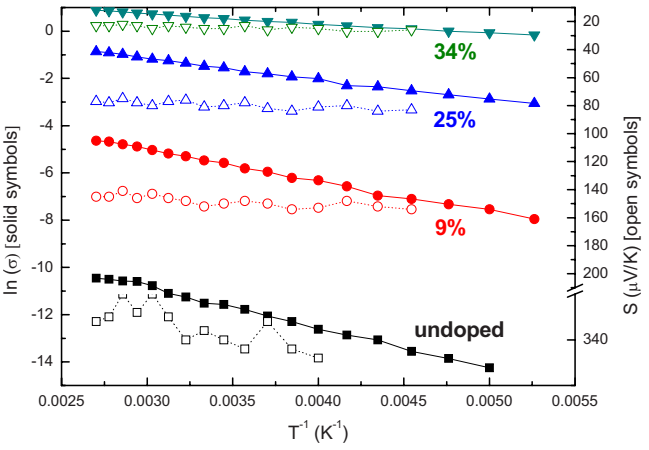

FIG. 4. (Color online) Temperature dependence of electrical conductivity (filled symbols) and Seebeck coefficient (open symbols) for various doping level.

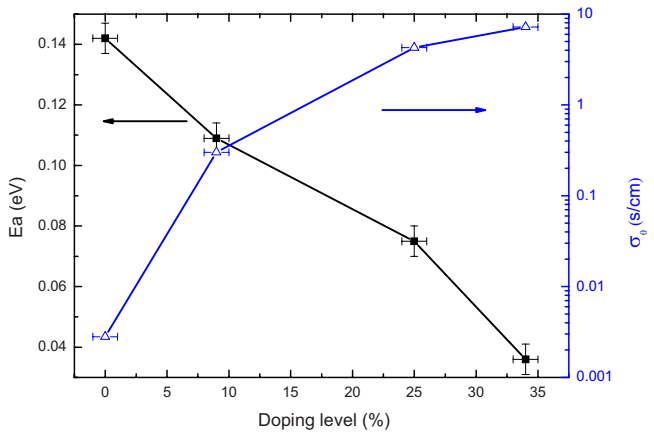

FIG. 5. (Color online) Evolution of the activation energy E_a (solid squares) and the pre-exponential factor σ_0 (open triangles) versus doping level.

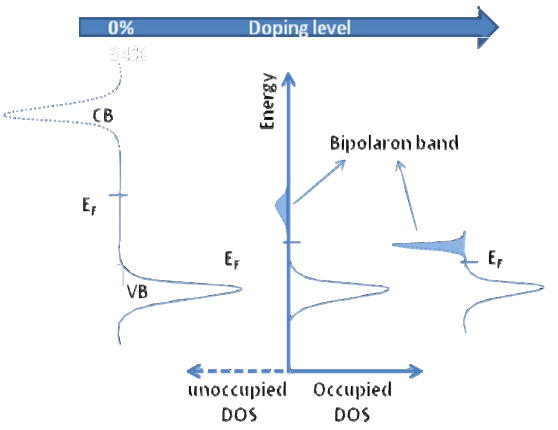

FIG. 7. (Color online) Schematic of the density of states in pristine and doped P3HT films. CB and VB denote the conduction and valence bands of the pristine P3HT.

doping has a much greater effect on the measured conductivity than it would be if each dopant just provided a charge carrier. In particular, if each dopant just contributes a carrier to the conductivity, its pre-exponential factor would be proportional to $\sqrt{c}$ as indicated in Eq. (8); and thus it would rise relatively slowly with the carrier concentration, as depicted in Fig. 6. Even the introduction of the doping dependence of the activation energy extracted from Fig. 4, $E_a=0.14-0.3c$ with $c<0.47$, produces a weaker doping dependence of the conductivity than the experimental data. This remaining discrepancy is attributed to the doping dependence of the transfer probability P.

Beyond adding positively charged carriers, dopants introduce PF_6^- counterions. Their irregular spatial distribution produces a disordered environment that charge carriers must traverse. Such disorder diminishes with increasing doping as the environment becomes progressively homogenized.[38]

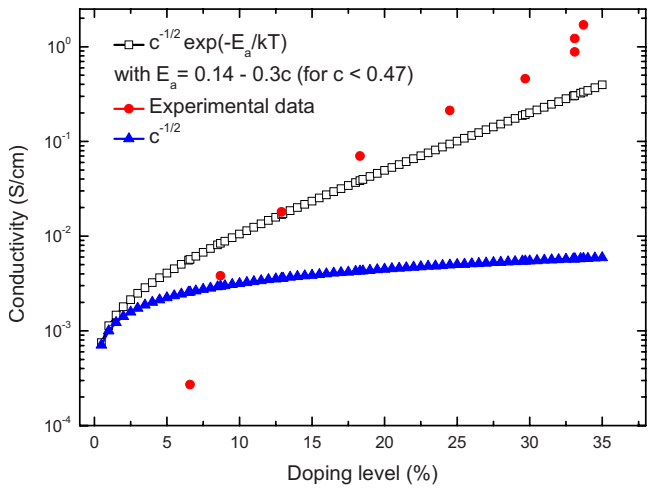

FIG. 6. (Color online) Evolution of the electrical conductivity (at room temperature) with the doping level and a comparison with theoretical trends using Eq. (8). The discrepancy between the rate of change of the conductivity between the open square and the experimental data (dots) is attributed by the variation in electronic coupling between the bipolarons.

Thus, as depicted in Fig. 7, with increased doping the width of the bipolaron band located within the polymer fundamental energy gap diminishes.

Disorder affects the hopping mobility by altering (1) the energies of the initial and final sites and (2) the transfer energies of those hops. Increasing the dispersion of site energies has the net effect of increasing the activation energy. Indeed Fig. 5 shows that the activation energy increases as the doping is reduced and disorder is increased. The electronic transfer energy affects the magnitude of the jump rate. In particular, as discussed below Eq. (7), the jump rate is proportional to the value of P which for a nonadiabatic hop is proportional to the square of the electronic transfer energy. The electronic transfer energies are very sensitive to the distance between the sites, the intervening potential and, most importantly for nonspherical local wave functions, the relative orientations of the units involved in the hop.[39] The increase in electronic transfer energies could contribute to the rise of the conductivity pre-exponential factor with increasing doping, as depicted in Fig. 5. The modification of the electronic transfer energy upon doping is supported by the change in chain packing visualized by the atomic force microscopy (AFM) measurements (Fig. 3).

All these results are thus consistent with localized positive bipolarons occupying a band of energies residing within the polymer fundamental energy gap (cf. Fig. 7). Transport occurs from p-type bipolaron hopping within the disordered environment produced by an irregular spatial distribution of counterions.

C. Seebeck coefficient

The Seebeck coefficients measured for samples having four different levels of intentional doping are plotted against $1/T$ in Fig. 4. Each of these Seebeck coefficients can be described as the sum of a constant term plus a relatively small contribution proportional to $1/T$. The magnitudes and slopes of these curves are plotted versus doping level in Fig. 8. The magnitude and slope of the Seebeck coefficients both decrease with increasing doping.

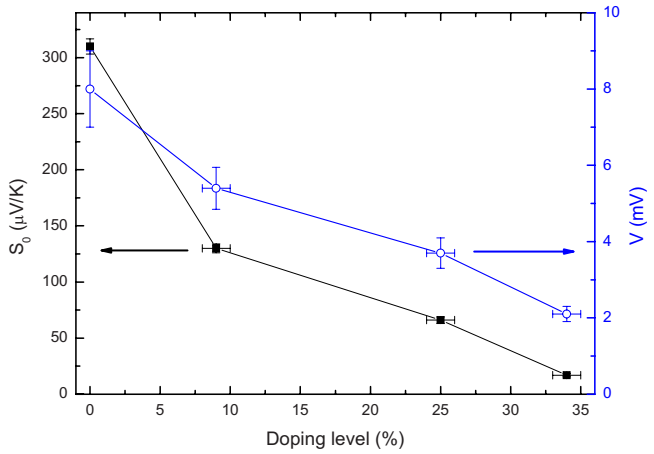

FIG. 8. (Color online) The evolution of the Seebeck coefficient's slope $\partial S/\partial(1/T)$ (V, the blue open circles) and its $1/T=0$ intercept (S_o, the black solid squares) with doping concentration.

These results are qualitatively different from those for inorganic semiconductors. The Seebeck coefficients of conventional semiconductors rise rapidly with increasing $1/T$ when the thermally stimulated carrier density decreases strongly. The slopes are typically at least several tenths of a volt. By contrast, the Seebeck coefficients of these doped polymers rise very slowly with increasing $1/T$. Indeed, the slopes are only 8 mV, 5.4 mV, 3.7 mV, and 2.1 mV for 0% (pristine), 9%, 25%, and 34% doping, respectively. In addition, the temperature-independent contributions to the Seebeck coefficients of doped P3HT are distinctive in that they vary strongly with doping.

Figure 9 shows that the doping dependence of the temperature-independent contributions to the Seebeck coefficients resembles that obtained when each dopant is presumed to contribute to one positive charge of the bipolaron, $c=2c_b$

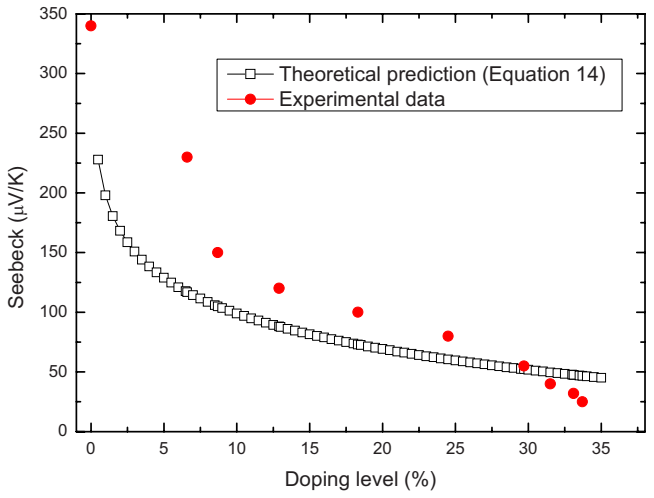

FIG. 9. (Color online) The comparison of the theoretical trend (open squares) of evolution of Seebeck coefficient vs doping level and the experimental data (filled circles) at room temperature.

$$S \cong \frac{k}{2q}\ln\left(\frac{1-c_b}{c_b}\right). \tag{14}$$

Here the Seebeck coefficient for bipolaron hopping in an ideal crystal, Eq. (10), has been simplified by ignoring pair breaking: pair breaking enhances the Seebeck coefficient by an amount that is greatest at low bipolaron concentration.

When a carrier hops between inequivalent sites of a disordered material some fraction of the energy exchanged with phonons is transported with it.[24] This fraction depends on the difference between the effective electron-phonon couplings at the hop's initial and final sites. The effective electron-phonon coupling of a site usually correlates with its energy. For example, a low-energy small-radius electronic state is more strongly coupled to phonons than is a higher energy larger radius electronic state. As a result some vibrational energy is transferred with a carrier as it hops through a disordered material. This energy, a fraction f of the activation energy of the carrier's mobility E_μ, contributes to the Seebeck coefficient[24]

$$S = \frac{k}{2q}\left[\ln\left(\frac{1-c_b}{c_b}\right) + f\frac{E_\mu}{kT}\right]. \tag{15}$$

As indicated in Fig. 8 and in the text above, the Seebeck slopes measured on our doped polymers are small and decrease with rising dopant level. These findings are consistent with dopants producing modest energetic disorder that is smoothed out with increased doping. Theoretical model for the Seebeck coefficient based on a percolation model of charge transport using a Gaussian density of state predicts this trend too: the slope of the Seebeck versus temperature is related to the width of the Gaussian distribution, i.e., to the degree of disorder.[40] The weakness of the Seebeck coefficient temperature dependence compared with that of the conductivity confirms a hopping-type mobility.[41,42]

The Seebeck coefficient and the electrical conductivity both generally vary with the carrier concentration. As a result, plotting a semiconductor Seebeck coefficient against the logarithm of the conductivity produces a pear-shaped figure.[43] Near-linear curves are produced in those portions of the figure in which carriers are primarily extrinsic. Indeed, a near-linear relation between S and $\log\sigma$ emerges from our treatment of bipolaron hopping within the Holstein-Hubbard molecular-crystal model (MCM). In particular, Eq. (14) yields $S \propto -\ln(\sqrt{c})$ for $c \approx 2c_b \ll 1$ while Eq. (8) gives $\sigma \propto \sqrt{c}$. Figures 6 and 9 show that the doping dependences of S and σ measured for our disordered material are much stronger than those predicted for the MCM. Nonetheless, Fig. 10 shows that our data produces a linear relationship between $\log\sigma$ and S. Linear relationships have also been found for polyaniline and polypyrrole.[8,44]

D. Thermoelectric power factor P_T

Figure 11 shows the evolution of the room-temperature Seebeck coefficient S, electrical conductivity σ and thermoelectric power factor $P_T \equiv S^2\sigma$ with doping. The conductivity of the P3HT film increases from 10^{-6} S/cm to 1 S/cm as the doping rises to its maximum. Concomitantly the positive

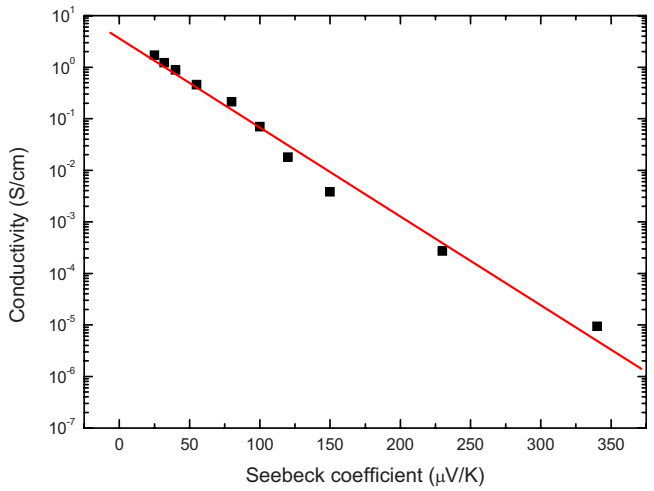

FIG. 10. (Color online) Log (conductivity) vs Seebeck coefficient for P3HT films at various doping levels at room temperature.

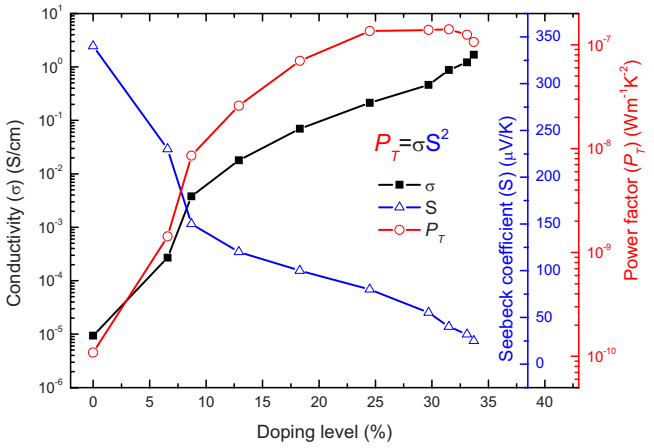

FIG. 11. (Color online) Doping dependence of the room-temperature Seebeck coefficient S (open triangles), electrical conductivity σ (filled squares), and thermoelectric power factor P_T (open circles).

Seebeck coefficient decreases from 340 to 25 μV/K. As a result the thermoelectric power factor $P_T \equiv S^2\sigma$ rises about three orders of magnitude from 10^{-10} W m^{-1} K^{-2} to achieve a broad maximum of $\sim 1.4 \times 10^{-7}$ W m^{-1} K^{-2} when the doping is increased in between 20% and 31%. As comparison, the power factor of Bi_2Te_3 is about 2×10^{-4} W m^{-1} K^{-2}.[45]

IV. CONCLUSION

The electrical conductivity and Seebeck coefficient of the conducting polymer P3HT are very sensitive to the doping produced through its reaction with the oxidant $NOPF_6$. This reaction yields positively charge carriers and PF_6^- counterions. Electronic transport requires the electronic charge carriers to navigate through the disordered environment induced by the presence of the counterions. Increasingly heavy doping progressively mitigates the localizing effects of the counterions and decreases the disorder. The electrical conductivity then rises sharply while the Seebeck coefficient falls. The importance of the disorder in conducting polymer explains both the decreasing activation energy of the conductivity as well as the weak temperature dependence of the Seebeck coefficient at high doping level. As a result the thermoelectric power factor reaches a broad maximum at between 20% and 30% doping.

ACKNOWLEDGMENTS

The authors gratefully acknowledge The Swedish Energy Agency and the Swedish Foundation for Strategic Research (SSF) supporting the research at Linköping University. The research in Mons is supported by the European Commission and Région Wallonne FEDER program (Materia Nova), by the Interuniversity Attraction Pole program of the Belgian Federal Science Policy Office (PAI 6/27), by the SOLWATT program of Région Wallonne (SUNTUBE project), and by FNRS-FRFC. J.C. and P.L. thank the Belgian National Fund for Scientific Research (FNRS).

[1] A. B. Kaiser, Adv. Mater. **13**, 927 (2001).
[2] A. B. Kaiser, Phys. Rev. B **40**, 2806 (1989).
[3] W. Rehwald and H. G. Kiess, *Conjugated Conducting Polymers* (Springer-Verlag, Berlin, 1992).
[4] C. M. Bhandari and D. W. Rowe, *CRC Handbook of Thermoelectrics* (CRC Press, Boca Raton, 1995.
[5] A. Shakouri and S. Li, Proceedings of the IEEE 18th International Conference on Themoelectrics, 1999 (unpublished), p. 402.
[6] F. Jiang, J. Xu, B. Lu, Y. Xie, R. Huang, and L. Li, Chin. Phys. Lett. **25**, 2202 (2008).
[7] X. Gao, K. Uehara, D. D. Klug, J. S. Tse, and T. M. Tritt, Phys. Rev. B **72**, 125202 (2005).
[8] N. Mateeva, H. Niculescu, J. Schlenoff, and L. R. Testardi, J. Appl. Phys. **83**, 3111 (1998).
[9] N. Toshima, Macromol. Symp. **186**, 81 (2002).
[10] Y. Shinohara, K. Hiraishi, H. Nakanishi, Y. Isoda, and Y. Imai, Trans. Mater. Res. Soc. Jpn. **30**, 963 (2005).
[11] S. Wakim, B. Aich, Y. Tao, and M. Leclerc, Polym. Rev. **48**, 432 (2008).
[12] F. Yakuphanoglu and B. F. Suenkal, J. Phys. Chem. C **111**, 1840 (2007).
[13] C. L. Kane and M. P. A. Fisher, Phys. Rev. Lett. **76**, 3192 (1996).
[14] H. Yan, T. Ishida, and N. Toshima, Proceedings of the IEEE 20th International Conference on Thermoelectrics, 2001 (unpublished), p. 310.
[15] R. Venkatasubramanian, E. Siivola, T. Colpitts, and B. O'Quinn, Nature (London) **413**, 597 (2001).
[16] M. Takeiishi, Proceedings of the 27th Japan Symposium on Thermophysical Properties, Kyoto, 2006 (unpublished).
[17] C. Wood, D. Emin, and P. E. Gray, Phys. Rev. B **31**, 6811 (1985).
[18] H. Shimotani, G. Diguet, and Y. Iwasa, Appl. Phys. Lett. **86**,

022104 (2005).
[19] S. Ukai, H. Ito, K. Marumoto, and S. Kuroda, J. Phys. Soc. Jpn. **74**, 3314 (2005).
[20] Y. H. Kim, D. Spiegel, S. Hotta, and A. J. Heeger, Phys. Rev. B **38**, 5490 (1988).
[21] R. Lazzaroni, M. Lögdlund, S. Stafström, W. R. Salaneck, and J. L. Bredas, J. Chem. Phys. **93**, 4433 (1990).
[22] J. Casado, V. Hernandez, S. Hotta, and J. T. Lopez Navarrete, J. Chem. Phys. **109**, 10419 (1998).
[23] K. Kaneto, S. Hayashi, S. Ura, and K. Yoshino, J. Phys. Soc. Jpn. **54**, 1146 (1985).
[24] D. Emin, Phys. Rev. Lett. **35**, 882 (1975).
[25] D. Emin, Phys. Rev. B **53**, 1260 (1996).
[26] S. A. Baily and D. Emin, Phys. Rev. B **73**, 165211 (2006).
[27] D. Emin and T. Holstein, Ann. Phys. (N.Y.) **53**, 439 (1969).
[28] D. Emin, *Electronic and Structural Properties of Amorphous Semiconductor*, edited by P. G. LeComber and J. Mort (Academic Press, London, 1973), pp. 261–328, Chap. 7.
[29] D. Emin, Phys. Today **35**, 34 (1982).
[30] N. Colaneri, M. Nowak, D. Spiegel, S. Hotta, and A. J. Heeger, Phys. Rev. B **36**, 7964 (1987).
[31] A. J. Heeger, S. Kivelson, J. R. Schrieffer, and W. P. Su, Rev. Mod. Phys. **60**, 781 (1988).
[32] G. Louarn, M. Trznadel, J. P. Buisson, J. Laska, A. Pron, M. Lapkowski, and S. Lefrant, J. Phys. Chem. **100**, 12532 (1996).
[33] M. Łapkowski and A. Proń, Synth. Met. **110**, 79 (2000).
[34] A. O. Patil and A. J. Heeger, Chem. Rev. **88**, 183 (1988).
[35] T. C. Chung, J. H. Kaufman, A. J. Heeger, and F. Wudl, Phys. Rev. B **30**, 702 (1984).
[36] D. Beljonne, J. Cornil, H. Sirringhaus, P. J. Brown, M. Shkunov, R. H. Friend, and J. L. Bredas, Adv. Funct. Mater. **11**, 229 (2001).
[37] J. A. Merlo and C. D. Frisbie, J. Phys. Chem. B **108**, 19169 (2004).
[38] V. I. Arkhipov, E. V. Emelianova, P. Heremans, and H. Bässler, Phys. Rev. B **72**, 235202 (2005).
[39] J. L. Bredas, J. P. Calbert, D. A. da Silva Filho, and J. Cornil, Proc. Natl. Acad. Sci. U.S.A. **99**, 5804 (2002).
[40] S. D. Baranovskii, I. P. Zvyagin, H. Cordes, S. Yamasaki, and P. Thomas, Phys. Status Solidi B **230**, 281 (2002).
[41] D. Emin, C. H. Seager, and R. K. Quinn, Phys. Rev. Lett. **28**, 813 (1972).
[42] Y. W. Park, A. Denenstein, C. K. Chiang, A. J. Reeger, and A. C. McDonald, Solid State Commun. **29**, 747 (1979).
[43] G. H. Jonker, Philips Res. Rep. **23**, 131 (1968).
[44] H. Yan, T. Ohta, and N. Toshima, Macromol. Mater. Eng. **286**, 139 (2001).
[45] J. Lee, Y. Kim, L. Cagnon, U. Gösele, J. Lee, and K. Nielsch, Phys. Status Solidi (RRL) **4**, 43 (2010).